Delft University of Technology

Document Version
Final published version

Citation (APA)

Important note
To cite this publication, please use the final published version (if applicable).
Please check the document version above.

Self-healing of cementitious materials using sustainable cenosphere-based manufactured aggregate

Leyang Lv [a], Xiangyu Zhang [a], Branko Šavija [b], Mingzhong Zhang [c], Kaihang Han [a], Honghzhi Zhang [d], Chun Pei [a,*], Jihua Zhu [a], Feng Xing [a]

[a] College of Civil and Transportation Engineering, Shenzhen University, Shenzhen 518060, China
[b] Microlab, Faculty of Civil Engineering and Geosciences, Delft University of Technology, 2628 CN Delft, the Netherlands
[c] Department of Civil, Environmental and Geomatic Engineering, University College London, London WC1E 6BT, UK
[d] School of Qilu Transportation, Shandong University, Jinan 25000, China

ARTICLE INFO

ABSTRACT

Self-healing concrete using encapsulated healing agent has shown great potential in enhancing concrete durability. However, the capsules are expensive to make and can lower the mechanical properties of concrete. In this study, a new type of manufactured aggregate that employs waste-derived fly ash cenosphere as a carrier of healing agent (SH-CS) was designed and produced. The effect of SH-CS incorporation on hydration, engineering properties and self-healing efficiency of cement mortar was systematically evaluated, with a special focus on self-healing mechanism through the analysis of the mineral composition of the healing product. The results indicate that the prepared SH-CS has good stability in and compatibility with cement mortar. The addition of SH-CS has small influence on the fresh properties of cement mortar and less negative effect on compressive strength at the hardened stage compared to the existing study. By replacing 3 wt.% of fine aggregate with SH-CS, up to 71% of the crack opening area of mortar specimens with a crack width of about 0.3 mm was self-healed after 28 days of water exposure. The self-healing behaviour of SH-CS led to a maximal 41% drop in water adsorption and contributed to the recovery of flexural strength. The healing products precipitated on the fracture surface were mainly composed of amorphous C-S-H and Calcite. It can be estimated that incorporating SH-CS in concrete would result in only a moderate (~29%) rise in cost for C40 concrete.

1. Introduction

Concrete cracking and crack-related durability issues can significantly impact the service life of concrete structures. Although cracks smaller than 200 μm are generally believed to have negligible impact on the performance of concrete, they may increase in size if not timely repaired. These cracks provide channels for the ingress of harmful agents such as chlorides [1] and CO_2 [2], which may lead to reinforcement corrosion and ultimately loss of serviceability of reinforced concrete [3]. Although manual repairing methods such as surface coating or grouting can help extend the service life of reinforced concrete structures to a certain extent, they are labour-consuming and cost-intensive. To tackle this issue, inspired by the biological self-healing phenomena, researchers proposed a novel concept for improving the durability of concrete, namely self-healing concrete [4–8].

To date, numerous studies have focused on endowing concrete with intrinsic repair ability by incorporating encapsulated self-healing agents as functional additives. With the successful development of microvascular [8–11] and microencapsulated healing agents [12], the recent research focus has shifted towards the development of self-healing manufactured aggregates that can be adopted as a replacement for natural aggregate in concrete. According to the material type of matrix, the manufactured aggregates can be divided into three categories: glass aggregate, polymeric aggregate and mineral-based aggregate. Glass tubes were first employed to convey silica gel or polyurethane immobilized bacteria in the realization of the intrinsic self-healing in concrete [13]. Following that, the self-healing effect of glass tubes encapsulating various types of liquid repair agents (sodium silicate, colloidal silica and polyurethane) and powder repair agents (magnesium oxide, bentonite and quicklime) were studied [14,15]. Although self-healing of concrete with encapsulated glass tubes has been demonstrated to be effective to some extent under laboratory

* Corresponding author.
E-mail address: ccpei@szu.edu.cn (C. Pei).

conditions, the limitations of glass aggregate in pervasiveness and survival ability in concrete are also obvious. To overcome this, polymers with various brittleness were used to produce macro or micro-sized polymeric capsules. The self-healing efficiency using polyurethane capsules was evaluated in terms of mechanical recovery and permeability [13,16]. Moreover, a chemical binding capacity of aggressive ions from seawater was realized using mineral encapsulated polymethyl methacrylate (PMMA) aggregate [17]. To better balance the survival ability and the triggering efficiency, Hilloulin et al. [18] investigated the feasibility of using polymeric capsules with different glass transition temperatures. Although the demonstration of the self-healing effect and survival ability in polymeric aggregates make it promise, a strong drawback is the weak compatibility of polymeric aggregates with the cementitious matrix that significantly reduces the fresh and hardened properties of the cementitious composites. In addition, the difference in density between polymer material and cement slurry makes the polymeric aggregate tend to suspend on the surface of freshly mixed slurry, which is not acceptable for field application. In viewing of this, mineral-based materials such as expansive clay [19,20], ceramics [21], and cementitious materials [22] were recently explored in manufacturing self-healing artificial aggregates. The reviewed literature shows that the mineral-based aggregates have good compatibility with cement matrix and are feasible to enhance the self-healing ability of concrete. However, most mineral-based aggregates for self-healing proposed to date require a complex manufacturing process and various commercial raw materials [23,24], resulting in relatively high costs that limit their widespread application in engineering practice. A recent study attempted to use recycled coarse aggregates (RCA) as carriers of microbial healing agents [25]. Specimens containing bacteria-immobilized RCA exhibited a significant self-healing effect. This study provides new thoughts on producing self-healing aggregates with waste-derived materials to reduce manufacturing costs and minimize consumption.

Fly ash cenosphere (hereinafter referred to as cenosphere) obtained from coal-fired power plants are hollow spherical particles, comprising aluminosilicates. The hardness of the cenospheres is up to 6–7 Mohs, with static compressive strength of up to 70–140 MPa. It was reported that adding cenospheres in different sizes to concrete can help reduce the demand for raw materials and density of concrete and improve the thermal insulation and crack resistance of concrete [26–29]. Recently, thanks to their unique hollow structure, the potential of using cenospheres as functionalized additives in cementitious materials has been explored [30]. Cenospheres loaded with water or phase change materials (PCMs) have been added to concrete to reduce shrinkage and increase the thermal energy storage capacity of concrete [31–33]. Incorporating cenosphere-based PCMs into concrete can enhance its building energy efficiency and cost-effectiveness while less impacting the mechanical properties [34,35]. Although the feasibility of using cenospheres as a functionalized carrier in concrete has been explored, the utilisation of cenospheres as a carrier of healing agent for self-healing cementitious materials has not yet been addressed.

In this study, waste-derived cenospheres were successfully converted into a new type of sustainable manufactured aggregate (SH-CS) to enhance the cost-effectiveness of existing self-healing strategies for cementitious materials. A three-step encapsulation technology was developed to impregnate the perforated cenospheres with the self-healing agent, while preventing the self-healing agent from leaking out of cenospheres during concrete mixing. The effect of the prepared SH-CS incorporation on the fresh and hardened properties of mortar was characterised. The self-healing efficiency of SH-CS in cementitious materials in terms of crack sealing effect, water absorption rate, and flexural strength regain was evaluated. A series of techniques including X-ray diffraction (XRD), thermogravimetry (TG), Fourier transform infrared spectroscopy (FTIR) and scanning electron microscope (SEM) were employed to explore the self-healing mechanism. In addition, to provide a reference to the industry for the potential application, the cost

of SH-CS and self-healing concrete was estimated.

2. Preparation and characterisation of self-healing cenosphere capsules

2.1. Materials

Sodium silicate (Na_2SiO_3) solution is used as a repair agent for cracked concrete. The repair mechanism involves the active reaction between silicate and calcium hydroxide in cement matrix, which forms hydrated calcium silicate (C-S-H gel) at the crack site[36], as described in Eq. (1). Lithium silicate (Li_2SiO_3) solution was applied on the surface of the impregnated cenospheres as a waterproof coating to prevent the unintentional leaking of the healing agent during the concrete mixing. The physical and chemical characteristics of the solutions are given in Table 1. Cenospheres with particle sizes ranging from 400–850 μm were adopted, the chemical compositions of which analysed using X-ray fluorescence (XRF) are presented in Table 2.

$$Na_2SiO_3 + Ca(OH)_2 \xrightarrow{H_2O} x(CaO \bullet SiO_2)H_2O + Na_2O \qquad (1)$$
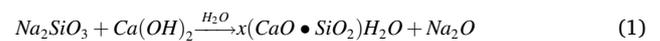
2.2. Manufacturing process

Cenonsphere-based self-healing manufactured aggregate (SH-CS) was developed through a three-step encapsulation process, as illustrated in Fig. 1. The encapsulation process of SH-CS started with perforating cenospheres with acid etching, followed by loading the healing agent into the perforated cenospheres using the vacuum negative pressure method, and encapsulating the loaded cenospheres with lithium silicate solution, as described below in detail.

2.2.1. Perforate cenospheres with acid etching (P-CS)

The shell of a cenosphere has a porous structure, making it an ideal carrier for self-healing agents. However, the shell of the as-received cenospheres is covered by a layer of nano-sized glass crystal film with high stiffness and hardness. To introduce liquid sodium silicate solution into the inner space of the cenospheres, the shell, must therefore be perforated to provide channels for the uptake of the healing agent. To this end, 0.3 kg of the as received cenospheres were exposed to 1 L of 1.2 mol/L hydrofluoric acid solution by immersing the dried microspheres into the acid etching solution. The volume ratio between the cenospheres and the hydrofluoric acid solution was about 1:3. Mechanical stirring (Fig. 1a) with a rotation speed of 60 r/min was applied to ensure that the surface of the hollow microspheres was entirely in contact with the acid etching solution. After stirring the solution for 2 h, cenospheres floated on the surface of the acid-etching solution were collected by passing the solution through #40 mesh sieves and rinsing the acid-etched cenospheres with water three times, followed by drying in an oven at 105 ℃ for 12 h.

2.2.2. Load sodium silicate into perforated cenospheres (NE-CS)

The healing agent, i.e., sodium silicate, was loaded into the perforated cenospheres by vacuum impregnation. More specifically, perforated cenospheres were first placed in a container in the vacuum tank (Fig. 1b). The internal pressure of the vacuum tank was then adjusted to

Table 1
Chemical and physical characteristics of sodium silicate and lithium silicate solution.

Material	Chemical formula	Mw (g/mol)	Density @ 20 ℃ (g/mL)	pH
Sodium silicate	$Na_2O(SiO_2)_x \bullet xH_2O$	122.06	1.39	12.5
Lithium silicate	$Li_2O(SiO_2)_x$	89.97	1.16	11

Table 2
Chemical composition (wt.%) of the as-received cenospheres.

Oxide	SiO_2	Al_2O_3	Fe_2O_3	K_2O	Na_2O	MgO	CaO	TiO_2	P_2O_5
Cenosphere	57.816	29.573	4.712	2.286	1.934	1.338	1.014	0.897	0.234
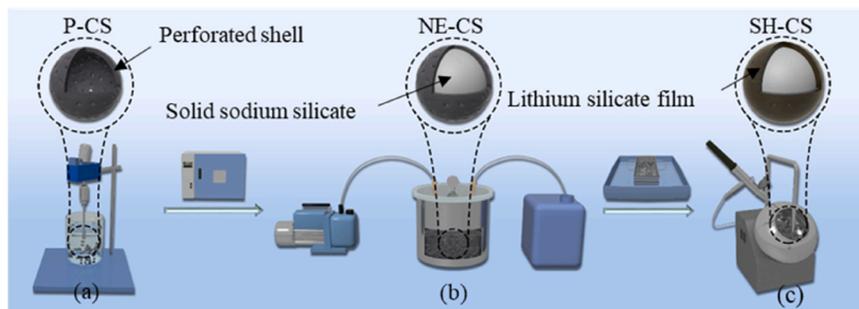
Fig. 1. Illustration of production process of SH-CS.

a vacuum pressure of −0.1 MPa and maintained for 1 h. Liquid sodium silicate was introduced into the container through a pre-set plastic pipe until the cenospheres were fully immersed in the solution. After the cenospheres were impregnated at −0.1 MPa for 0.5 h, the sodium silicate loaded cenospheres were filtered with a sieve, rinsed by tap water, and left to dry in a rotating granulator (Fig. 1c) for 3 h under hot air blowing at 60 ℃ and at a rolling speed of 60 r/min.

2.2.3. Coating sodium silicate loaded cenospheres with lithium silicate (SH-CS)

To prevent the unintentional leakage of the loaded healing agent from the perforated cenospheres, the loaded cenospheres must be encapsulated by a waterproofing layer. This was achieved by innovative coating of the cenospheres with lithium silicate solution. The coating was done by spraying the loaded cenospheres with lithium silicate solution in a rotating granulator under hot air blowing at 60 ℃ and a rolling speed of 60 r/min. The volume ratio between the loaded cenospheres and the lithium silicate solution was 5:1. To facilitate the formation of the waterproof film on the surface of cenospheres, the coated cenospheres were dried in the rotating granulator under hot air blowing at 60 ℃ for another 3 h. Finally, the sand-like SH-CS was collected from the rotating granulator and sealed in a plastic bag for further experiment.

2.3. Characterisation

2.3.1. Product appearance

The images of as-received cenospheres, perforated cenospheres (P-CS), sodium silicate loaded cenospheres (NE-CS), and the final product of SH-CS was recorded. Fig. 2 shows the images of SH-CS at various stages of preparation. There existed no significant difference between the as-received cenosphere, P-CS, NE-CS and SH-CS. The sand-like particles of SH-CS were believed to have a good dispersibility in the cement

matrix.

2.3.2. Particle size distribution

The particle size distribution of SH-CS final product was characterised using laser particle analyzer (Matersizer 3000, Malvern Panalytical Ltd., USA), which is presented in Fig. 3. The size of the prepared SH-CS ranged between 370 and 1000 μm and the mean particle size of SH-CS is about 700 μm. The particle size distribution of SH-CS is similar to that of fine natural sand.
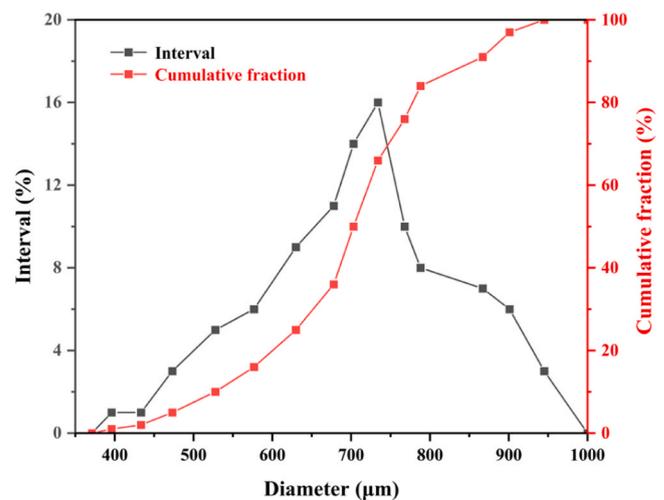
Fig. 3. Particle size distribution of SH-CS.
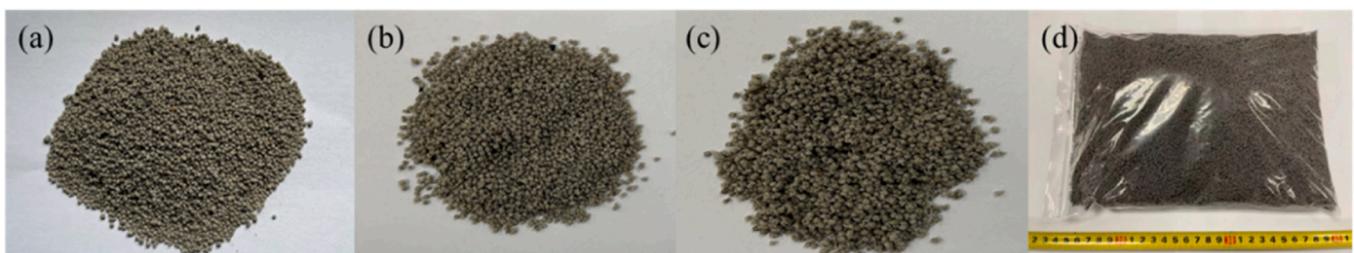
Fig. 2. Images of (a) as-received cenospheres, (b) P-CS, (c) NE-CS, and (d) SH-CS final product.

2.3.3. Morphology

The morphology of SH-CS was investigated using environmental scanning electron microscope (ESEM) (Quanta TM 250 FEG, FEI, United States). To improve the image resolution, the surface of the specimens was coated with gold prior to ESEM observations. Conductive tape was used to bind the particles on the sample holder. Fig. 4 displays the morphology of SH-CS at different stages of preparation. It is evident that, compared to the as-received cenospheres in Fig. 4(a), P-CS shown in Fig. 4(b) has been perforated. Pores with a diameter of about 10–30 μm can be observed on the outer surface of P-CS, indicating that the outermost glass crystal film covering the as-received cenospheres has been successfully removed through the acid etching treatment. It is generally believed that the porous structure of cenospheres could provide channels for introducing sodium silicate solution. Fig. 4(c) demonstrates the SEM image of NE-CS that was manually crushed before SEM imaging. The healing agent had been successfully impregnated and partially occupied the inner space of the hollow microsphere. Furthermore, the healing agent (sodium silicate) was closely attached to the shell of the cenosphere. To prevent the leakage of sodium silicate during the concrete mixing, which could possibly interfere with cement hydration, the last step in producing self-healing manufactured aggregate is to coat NE-CS with a layer of lithium silicate. Fig. 4(d) illustrates the morphology of the final product of SH-CS. Apparently, the surface of the SH-CS particle was covered with a dense layer, and the holes on the cenosphere have mostly been sealed.

2.3.4. Encapsulation effectiveness

Sodium silicate is a soluble substance, which can be dissolved into sodium and silicate ions when encountering water. The density of the dissolved ions in the solution can be characterised by the solution's conductivity. To verify the encapsulation effectiveness of the proposed self-healing manufactured aggregate, the conductivity of the water solution dispersed with P-CS, NE-CS and SH-CS was studied, the results of which are presented in Fig. 5. At the initial 60 min, the conductivity of the solutions dispersed with NE-CS and SH-CS increased significantly compared to the solution with P-CS. This can be interpreted that both SH-CS and NE-CS existed to some extent of leakage with the impregnated healing agent. However, the conductivity of SH-CS solution at 60 min was only about 445 μs/cm, which is much lower than that of NE-CS, 1440 μs/cm. Furthermore, the conductivity of SH-CS solution
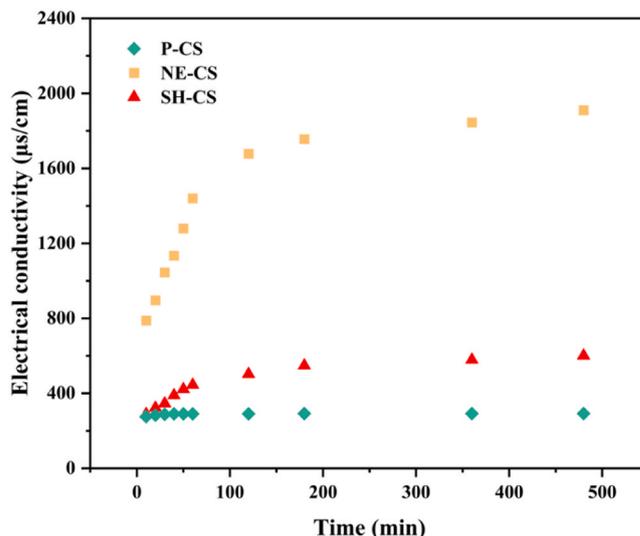
Fig. 5. Electrical conductivity of water solution dispersed with P-CS (Ref), NE-CS and SH-CS, respectively.

tended to be stable at 600 μs/cm after 180 min of exposure, while the conductivity of NE-CS continued to grow. These results indicate that the encapsulation of NE-CS with lithium silicate can effectively protect the repair agent from leaking out of the carrier in concrete slurry.

3. Experimental program

3.1. Raw materials

Commercial ordinary Portland cement (CEM I 42.5 N) was used in

Table 3
Chemical composition (wt.%) of Portland cement.

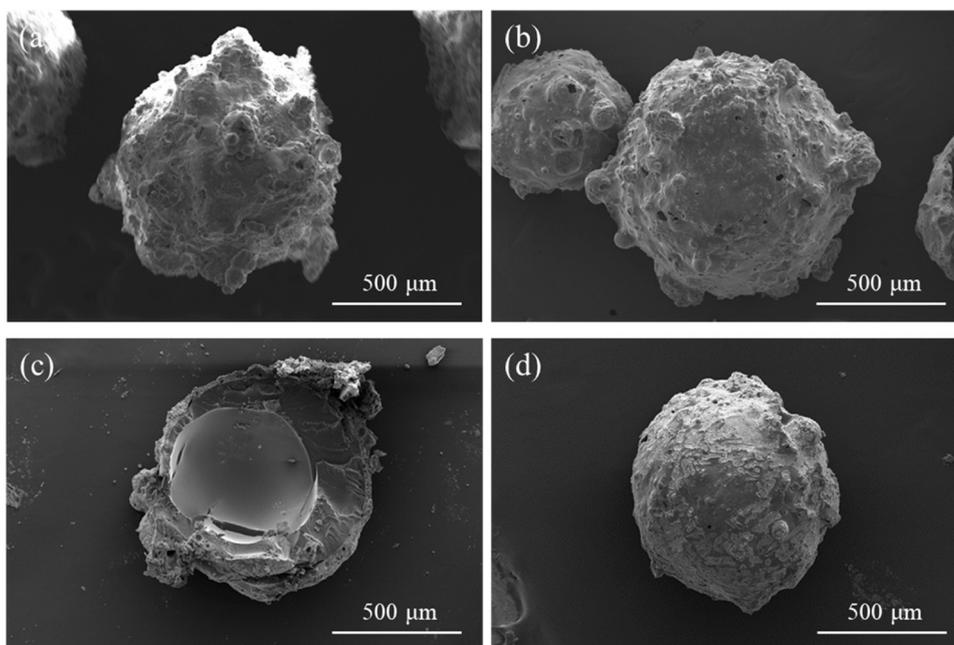| Oxide	CaO	SiO_2	Al_2O_3	Fe_2O_3	SO_3	MgO	Others
Cement	63.75	21.91	4.82	3.18	3.29	2.40	0.67

Fig. 4. SEM images of (a) as-received cenospheres, (b) P-CS, (c) NE-CS and (d) SH-CS final product.

this study, the chemical composition of which is given in Table 3. CEN Standard sand as per EN 196–1 [37] was adopted as fine aggregate and tap water was used as the mixing water.

3.2. Mix proportions

The weight ratio of water, cement and sand of cement mortar was 1:2:6. The prepared manufactured aggregate (SH-CS) was incorporated as a replacement for 3 wt% of sand in the mixture (SH_3%), considering the balance of a good self-healing effect and no significant drop in workability of cement mortar. For comparison, the control sample (Ref) and the samples with 3 wt% of P-CS (P-3%) and with 3% NE-CS (NE-3%) were also studied. Given the similar density of sand and encapsulated cenosphere, the weight ratio instead of the volume ratio was adopted here. No other additive was used in the mix to avoid interference in the results. The mix proportions of mortar specimens studied are presented in Table 4.

3.3. Sample preparation

Besides the hydration heat test where cement paste was applied, mortar was mixed for the rest of test according to the mix proportions given in Table 4. After a regular mixing procedure, the resulting fresh mortar was used for the workability and setting time test. Mortar specimens for dry shrinkage and compressive were cast using $40 \times 40 \times 160$ mm moulds. A vibration table was applied to compact the mortar specimens. After sealed curing in lab condition for 24 h, the specimens were de-moulded and placed in a fog room for further curing until 28 d.

Mortar specimens for the self-healing efficiency test were cast as follows. First, a layer of 10 mm mortar was poured into the 40 mm $\times$ 40 mm $\times$ 160 mm moulds. Then, two steel reinforcing bars with a diameter of 1.5 mm were placed on the surface of the mortar layer. The steel bars were used to control the crack opening during crack formation. After positioning the reinforcing bars, the remainder of the moulds was filled with mortar. After casting, the moulds were wrapped with plastic film and stored at lab condition (23 °C, 50% RH) for 24 h. Subsequently, the samples were de-moulded and delivered to standard curing conditions (20 °C, 98% RH) for another 27 d. A universal testing machine (RGM-4020, Shenzhen Tiger Instrument Co. Ltd., China) coupled with a three-point bending test module was applied to the hardened specimens to introduce cracks. Displacement was applied at a continuous rate of 0.1 mm/min. A portable concrete crack detector monitored the average width of the crack in real time (BJLF-1, Beijing Institute of Optoelectronic Technology, China). The loading process was stopped once the crack width reached the target value (0.3 mm in this study). Since crack closure occurs upon unloading, the specimens with a crack width less than 0.3 mm were loaded again to expand further the damage to a crack width 10% higher (i.e., 0.33 mm) until the residual crack width reached the target value. Three cracked samples were selected in each group, and 5 marker points were chosen on the cracking surface of each sample to measure their crack width.

3.4. Testing methods

3.4.1. Hydration heat test

The effect of cenosphere incorporation on the hydration heat of

Table 4
Mix proportions of mortar specimens (%).

Sample ID.	Water	Cement	Sand	P-CS	NE-CS	SH-CS
Ref	11.1	22.2	66.7	0	0	0
P_3%	11.1	22.2	64.7	2	0	0
NE_3%	11.1	22.2	64.7	0	2	0
SH_3%	11.1	22.2	64.7	0	0	2

cement paste was measured using an isothermal calorimeter (TAM Air 8-channel, TA Instruments, USA) according to ASTM C1702–09 [38]. To investigate the addition of cenospheres at various producing stage on the hydration kinetics of cement paste, P-CS, NE-CS and SH-CS was added by replacing 9 wt.% of cement powder in the mixture. The hydration heat of pure cement paste was also tested as a reference. To ensure the accuracy of the test, the mix water was stored in the lab for 24 h before it was applied to the mixing procedure. The water-to-cement ratio of cement paste is 0.5. All cement mixtures were mixed in a pan mixer and poured into a glass ampoule bottle that was specially fitted to the channel of the calorimeter. The mixed cement paste subjected to the test was taken 10% out of a 100 g well-mixed cement paste batch. This means that each ampoule bottle contained 10.0 g of mixed cement paste. Before the test, the calorimeter was adjusted to a constant temperature of 22 ± 1 °C and equilibrated for 24 h. The heat evolution of the cement paste was recorded continuously for 7 d. A factor of 0.91 was applied to the results of the pure cement paste (Ref) to ensure that the weight of cement is consistent with each of test.

3.4.2. Workability test

The workability of each mix was determined as per ASTM C1437 [39]. A cone mould with an upper inner diameter of 70 mm, a lower inner diameter of 100 mm, and a height of 60 mm was placed at the centre of a clean and level glass plate. The freshly mixed mortar was poured into the cone mould in two stages. Firstly, the mortar was poured into the mould to a height of two-thirds of its depth, and then it was compacted uniformly for 15 times from the edges to the centre using a compacting hammer. Secondly, the mortar was poured to a height approximately 20 mm above the mould, and it was compacted uniformly 10 times in the same manner. After the compaction, excess mortar on the surface of the mould was removed using a steel spatula. The test mould was then lifted vertically, and a vibrating table was started followed by 25 cycles of vibration at a frequency of one cycle per second. After completion of the vibration, callipers were used to measure the diameters of the mortar's bottom surface in two perpendicular directions.

3.4.3. Setting time test

Automatic Vicat apparatus (Vicatromic, Matest Co., Ltd. Italy) was applied to characterise the setting time according to ASTM C191[40]. The initial setting time was obtained when the needle penetrated the cement paste for 25 mm. The final setting time was attained when there was no mark of the specimen surface with a complete circular impression. To ensure the precision of the evaluation result, the tests were repeated three times for each specimen.

3.4.4. Dry shrinkage test

The dry shrinkage of mortar specimens was measured as per EN 12617–4 [41]. Freshly mixed mortar was first poured into standard-sized moulds ($40 \times 40 \times 160$ m³) with fixed anchor. After 1 d of curing under standard laboratory conditions, the specimens were de-moulded and then placed in a controlled environment at constant temperature of 20 ± 2 °C and a relative humidity of $60 \pm 5\%$ for another 27 d. The lengths of the specimens were measured at curing ages of 1, 3, 7, 14, 21, and 28 d respectively using a cement paste length comparator. Subsequently, the drying shrinkage of the specimens was calculated for each age as follows:

$$\varepsilon_x = \frac{L_0 - L_x}{160} \tag{2}$$

where ε_x represents the drying shrinkage (dimensional change) at the age of x d, L_x is the length of the specimen at the age of x d, and L_0 is the initial length of the specimen.

3.4.5. Compression test

To investigate the effect of cenosphere-based manufactured aggregates incorporation on the mechanical properties of the mortar, the compressive strength of the prepared mortar specimens was measured as per ASTM C109 [42]. Each of the data was obtained on an average of 3 replicate tests.

3.4.6. Self-healing efficiency evaluation

3.4.6.1. Triggering effect.
The rupture of the SH-CS upon cracking is the prerequisite to the realization of self-healing function of SH-CS in concrete. Therefore, to prove the feasibility of applying the as-prepared self-healing manufactured aggregate in concrete, the fracture surfaces of the specimens generated in the compressive strength test were observed using an optical microscope (OM) to verify the rupture of the SH-CS upon crack.

3.4.6.2. Crack healing.
To test the self-healing capability of the SH-CS at different stages of preparation in mortar, four series of specimens, Ref, P_3%, NE_3%, and SH_3% were prepared as described in Section 3.3. Following the crack introduction process, all the cracked specimens of P_3%, NE_3%, SH_3%, and Ref were subjected to the healing process by immersing the specimens in tap water at 20 °C. After healing in the water for 28 days, a stereo microscope was used to observe the crack healing effect and record the crack width change at the marker point. The following formula was used to calculate the crack healing rate:

$$\varphi = \frac{W_i - W_x}{W_i} \times 100\% \tag{3}$$

where φ denotes the crack mouth sealing ratio (%), W_i is the initial crack width (μm), and W_x is the crack width after healing for 28 d (μm).

3.4.6.3. Water absorption.
According to the testing protocol described in ASTM C1585–13 [43], a modified water absorption test described in a previous study [44] was performed on the healed specimens, i.e., Ref, P_3%, NE_3%, and SH_3%. The Ref specimens were used as a reference for the maximum water absorption capability of cracked mortar. Before the test, the specimens were placed in a drying oven at a temperature of 40 ℃ for three days to remove the moisture. Then, the surface of the specimens where contact with water was sealed with adhesive aluminium tape, except for the crack mouth and adjacent area. The initial mass of the sealed specimens was measured to an accuracy of 0.01 g and was recorded to calculate the water absorption rate. Following that, two supports (reinforcing bars were used as supports in this case) were placed parallel to the bottom of the water tank. The water tank was filled with tap water, with the water level 3 mm above the top of the supports. Once the test surface of the specimens was placed on the supports, the timer was started immediately. The time and weight were recorded at 60 s, 5 min, 10 min, 20 min, 30 min, and every hour until 4 h soon after the specimen immersed in water. The water absorption rate (I) can be calculated as:

$$I = \frac{m_t}{a \times b} \tag{4}$$

where the absorption rate, I, is defined as the change in mass in grams (m_t) divided by the cross-sectional area of the test specimen (a, mm^2) and the density of water (b). Since the change in water density is neglected, a constant value of 0.001 g/mm^3 was used for b. The sorptivity index (S, mm/s$^{1/2}$) is defined as the slope of the line that best fits the absorption I plotted against the square root of time (s$^{1/2}$). This slope was obtained using least squares, linear regression analysis of the plot of I versus square root of time (s$^{1/2}$). All the points from 1 min to 4 h were used for the regression analysis. For each data point, three replicate samples were tested.

3.4.6.4. Mechanical recovery.
The flexural strength of the uncracked specimens (first round) and the cracked specimens healed in water for 28 d (second round) was tested to characterise the mechanical recovery performance of SH-CS in mortar. It should be noted that the specimens tested here are mortar specimens with two steel bars embedded. In the first round, the specimens were pre-cracked and the flexural strength for each batch of specimens was recorded. After healing in water for 28 d, the healed specimens were tested for the second round until failure. Due to the presence of steel bars, the flexural strength obtained from the second-round test of Ref specimens was regarded as the residual strength, which includes the pull-out strength of the steel bars and the strength resulting from the further hydration cement matrix. This value should therefore be excluded when calculating the mechanical recovery rate of the healed specimens. The flexural strength recovery rate (F_{sr}) resulted from the self-healing effect can be calculated as:

$$F_{sr} = \frac{f_2 - f_{Ref}}{f1} \times 100\% \tag{5}$$

where f_1 is the flexural strength for the virgin specimen (first round three-point bending test), f_2 is the flexural strength for the healed specimen (second round three-point bending test), and f_{Ref} is the residual strength of Ref sample.

3.4.6.5. Healing mechanism.
To reveal the healing mechanism of SH-CS in concrete, the chemical composition of the repair products at the fracture surface was characterised using XRD, FTIR, TGA and ESEM. For XRD, TG, and FTIR analysis, the repairing product was first collected with a file by scraping the repairing product from the fracture surface of the 28 d healed specimens and then ground in a corundum mill for 15 min. To prevent any further reaction, the powder of the repairing product was immersed in acetone for 24 h and then filtered by vacuum to extract the acetone. Finally, the filtrate was dried in an aerated oven at 60 °C for 24 min and vacuum sealed in a plastic sample bag until the test.

XRD analysis was performed using a Bruker D8 in a θ - 2θ configuration with a monochromatic CuKα radiation equipped with the LYNXEYE detector. The voltage and the current of the generator were set to 40 kV and 40 mA, respectively. The 2θ range of the measurement was set to 5° to 80° with a step size of approximately 0.02°. The FTIR spectra of the samples were collected using an FTIR (Nicolet IS5, Thermo Fisher Scientific Inc.) in transmission mode in the spectral range of 4000–600 cm^{-1} and a resolution of 1 cm^{-1}. TG analysis was conducted using a thermogravimetric analyser (STA6000, Perkin Elmer Inc.) under flowing nitrogen (40 mL/min). The temperature was increased from 30 to 1000 ℃ at a heating rate of 10 ℃/min. The microstructure of the healing product was directly observed on the fractured surface of the healed specimens using an environmental scanning electron microscope (Quanta TM 250 FEG, FEI, United States) with an acceleration voltage of 10 kV.

4. Results and discussion

4.1. Hydration heat

Fig. 6 presents the heat evolution and the accumulative heat of pure cement paste (Ref specimens) and cement paste containing 9% of P-CS, NE-CS and SH-CS, respectively. As seen in Fig. 6a, the total heat released from NE-CS specimens was generally higher than that of the rest of specimens. This can be attributed to the leaking of sodium silicate from the NE-CS into the cement slurry as the NE-CS is not coated with a waterproofing layer. The leaked sodium silicate reacted with calcium hydroxide in the cement slurry, which promotes the formation of C$_3$S and, therefore, generates more hydration heat during the first 100 h of cement hydration. Previous studies have also reported that the hydration rate of Portland cement could be promoted after including sodium
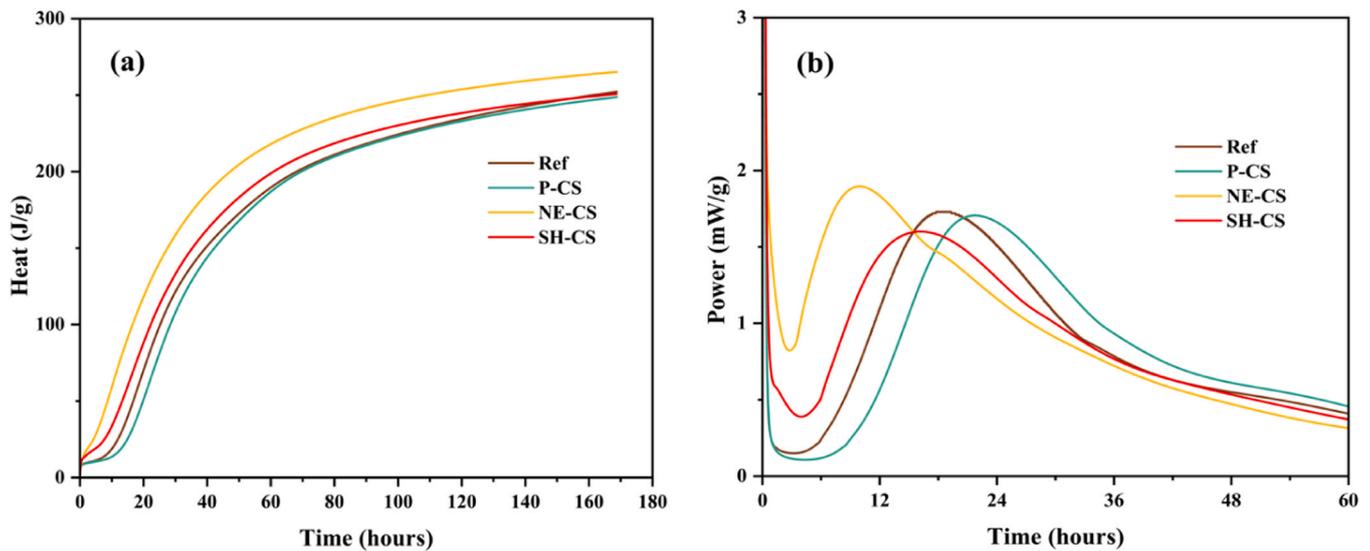
Fig. 6. Effects of P-CS, NE-CS and SH-CS incorporation on (a) total heat of hydration, and (b) rate of heat evolution during hydration.

silicate in the cement mixture [45,46]. Although the accumulative hydration heat of Ref, P-CS and SH-CS mixed sample is almost the same at the end of test, the hydration heat released by the specimen mixed with SH-CS is significantly lower than that of the sample mixed with NE-CS. This proves that the encapsulation of NE-CS with lithium silicate coating can effectively protect the sodium silicate from leaking out of the cenospheres to the matrix during mixing.

The heat release rate of cement paste specimens with and without various types of cenosphere is shown in Fig. 6b. Compared with NE-CS, P-CS and Ref, the prominent exothermic peaks of SH-CS sample had the lowest value in the exothermic rate, suggesting that the inclusion of SH-CS could, to some extent, reduce the heat releasing rate of cementitious materials. In contrast, the exothermic rate of cement containing NE-CS was apparently higher than other specimens and shifted to the left, as releasing sodium silicate from NE-CS promotes hydration. It is also interesting that the exothermic peak of P-CS samples shifted to right of Ref, which can be ascribed to the less water available for cement hydration as part of the mixing water was absorbed to wet the surface of P-CS [31].

4.2. Workability

Fig. 7 illustrates the workability of each mortar mix. The P_3% group exhibited the highest workability (231 mm), which is 2.7% higher than the Ref sample. This can be attributed to the inclusion of spherical microspheres, which reduces the friction between sand particles and the cement matrix, thus reducing the cohesion of the slurry and consequently enhancing its flowability. As for NE_3%, due to the absence of encapsulation, sodium silicate in NE-CS is prematurely mixed into the cement slurry. The chain-like structural tetrahedral ion groups in sodium silicate that bonded with calcium in the cement reduces the flowability of the cement slurry. As a result, the flowability of NE_3% mortar decreased by 20% compared to the control group. In contrast, the flowability of the SH_3% group mortar only decreased by 6.7% compared to the control group, indicating that the addition of SH-CS into the slurry did not significantly impact the workability of cement mortar.
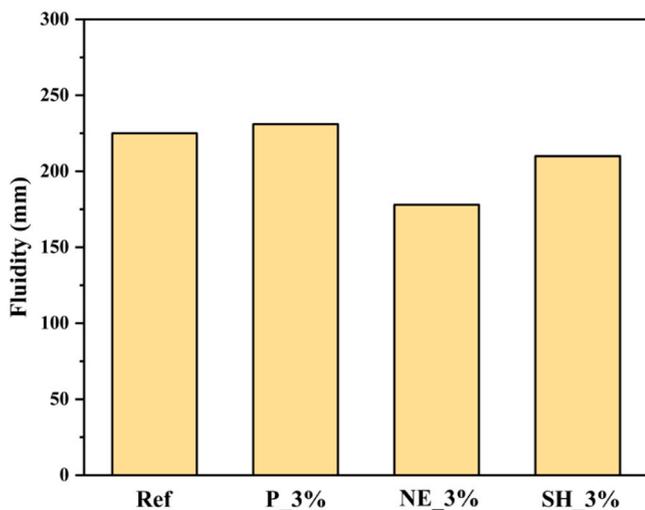

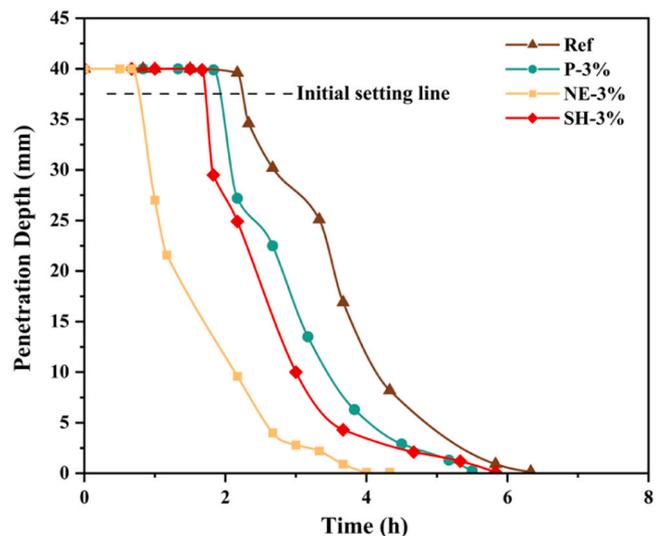**Fig. 7.** Fluidity of Ref, P_3%, NE_3% and SH_3%.

Fig. 8. Effect of different aggregates incorporation on the setting time of mortar.

4.3. Setting time

Fig. 8 shows the setting time for Ref, P_3%, NE_3% and SH_3%. Based on these curves, the initial and final setting time for each of these specimens is given as follows: Ref - 2.2 h and 6.3 h, P_3% - 1.9 h and 5.5 h, NE_3% - 0.8 h and 3.8 h, and SH_3% - 1.7 h and 5.8 h, respectively. The incorporation of NE-CS showed the most significant effect in shortening the initial and final setting time of mortar. This can be attributed to the unintentional leakage of the healing agent, sodium silicate, into the cement matrix. The sodium silicate with high alkalinity could dissolve in the mixing water during the mortar setting and became an accelerator to the hydration process, as previously documented [45]. Unlike the specimens incorporated with NE-CS, the accelerating effect of P-CS was originated from the decreased water-to-cement ratio as the P-CS absorbed part of the water, which should have participated in the cement hydration. A previous study reported that a lower water-to-cement ratio resulted in the acceleration of cement hydration [47]. In line with result of hydration heat, the setting time of cement mortar is only slightly shortened by the inclusion of SH-CS. Compared to Ref, the initial and final setting time of SH_3% specimens were retarded by about 0.5 h. The results presented here demonstrate that the incorporation of SH-CS has a negligible effect on the setting time of mortar and can be incorporated safely as manufactured aggregate.

4.4. Dry shrinkage

The drying shrinkage of mortars containing P-CS, NE-CS, SH-CS, and the control group is presented in Fig. 9. Among all sample groups, P_3% exhibited the lowest value of drying shrinkage, ending at 291.67 με at 28 d. The reduction in drying shrinkage can be ascribed to the absorption of water by P-CS that reduced the total water available for cement hydration, consequently lowering the drying shrinkage of the specimens. This observation aligns with the findings by Feng et al. [33]. In comparison to the control group, the drying shrinkage of NE_3% and SH_3% groups at 28 d of curing increased by 52.9% and 29.4%, respectively. Both of two groups exhibited higher value of drying shrinkage, which can be attributed to the increase in the porosity of the mortar system due to the pre-releasing of sodium silicate that facilities the evaporation of free water within the system.

4.5. Compressive strength

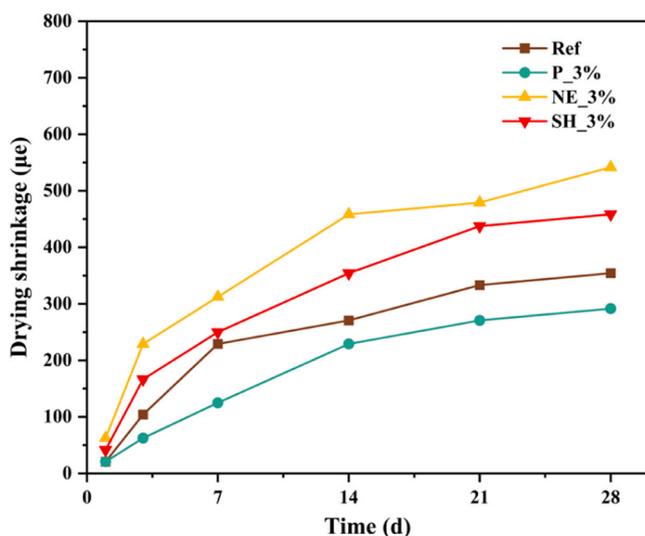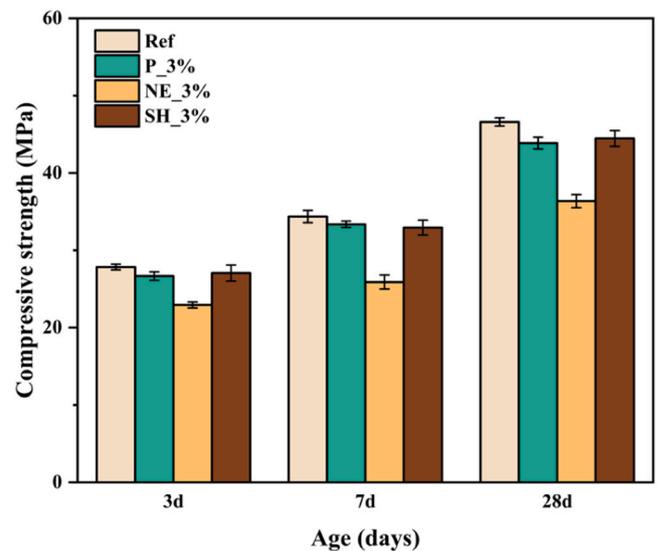Fig. 10 shows the compressive strength of mortar samples with P-CS,

Fig. 10. Compressive strengths of blank mortar (Ref) and mortar with P-CS, NE-CS and SH-CS.

NE-CS, and SH-CS at 3, 7, and 28 d. Although the compressive strength increased with curing age, Ref exhibited the highest compressive strength compared to P_3%, NE_3%, and SH_3% specimens. Specifically, P_3% showed an insignificant decrease in compressive strength compared to the reference specimen, which can be attributed to the lower compressive strength of the hollow cenospheres in the mortar specimens compared to sand particles [33,48]. Furthermore, a significant difference in compressive strength could be characterized by comparing Ref and NE_3%. A 22% lower compressive strength value than the Ref specimen was monitored on NE_3% at 28 days. It can be assumed that, soon after the release of sodium silicate from the NE-CS during cement hydration, the SiO_3^{2-} in the sodium silicate reacted with the Ca^{2+} in the slurry, resulting in the formation of calcium silicate hydrate (C-S-H gel) on the surface of cement particles. The generated hydration product filled between cement particles hindered the further hydration and strength development of cement. Similar phenomena were reported in [49,50]. As for SH_3%, mortar specimens with SH-CS exhibited significantly higher compressive strength compared to the NE_3% specimen at the hydration age of 3, 7 and 28 d. This means that encapsulating NE-CS with lithium silicate can effectively avoid the unintentional release of sodium silicate.

To further illustrate the impact of the self-healing agent inclusion on the mechanical strength of cementitious materials, the 28 d compressive strength of SH_3% reported in this study was compared with those of mortars containing self-healing agent at the same or similar weight ratio. As shown in Fig. 11, the strength reduction of SH_3% was the lowest in comparison with other reported encapsulation methods [16, 23,24,51–54]. This comparison confirms the excellent mechanical performance of the prepared self-healing manufactured aggregate in mortar.

4.6. Self-healing efficiency

4.6.1. Rupture of SH-CS upon crack

The self-healing function of the prepared manufactured aggregate is reached through the rupturing of cenosphere particles. To this end, the specimens of SH_3% were fractured and then subjected to OM to visualize the rupture behaviour of SH-CS upon crack. The fracture surface of the cementitious mortar embedded with SH-CS is shown in Fig. 12. It is evident from the image that the dried healing agent (sodium silicate) was appropriately stored in the cenosphere, indicated by the bright area in the inset image. Furthermore, the ruptured SH-CS has a firm
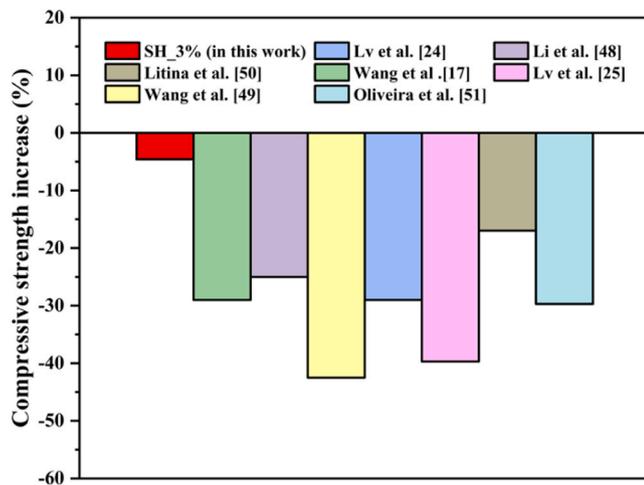

Fig. 9. Effect of different aggregates incorporation on the drying shrinkage of mortar.

Fig. 11. Comparison of 28 d compressive strengths of mortar containing SH-CS with the existing study containing other types of self-healing particles.
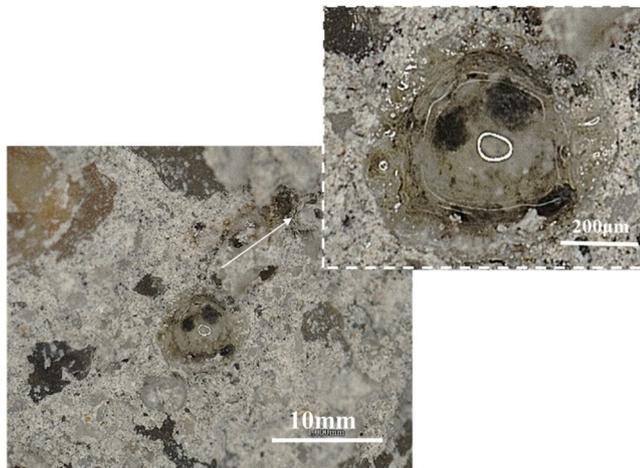

Fig. 12. OM images of the fractured surface of a mortar specimen with embedded SH-CS.

interlayer transition zone with the cement matrix, suggesting that the prepared SH-CS self-healing manufactured aggregate can protect the healing agent during the mixing and casting process while it can rupture during the crack propagation.

4.6.2. Crack sealing effect

The change in crack width is a commonly used index in characterising the self-healing ability of concrete [55,56]. Fig. 13 shows the initial crack width (X-axis) and the crack width after 7 and 28 d of healing in water (Y-axis). As depicted in Fig. 13a, Ref sample showed some extend of self-healing, with a roughly 10% reduction in crack width after 28 d of exposure to water. A prior study attributed this phenomenon to the further hydration of unreacted cement, leading to the formation of insoluble precipitates at the opening of the crack [57]. However, due to the limited amount of unhydrated substances, the self-healing ability of the Ref sample only became apparent primarily for cracks with widths ranging from 150 to 250 μm. The introduction of P-CS had a minimal impact on the self-healing ability of mortar (Fig. 13b), with crack repair performance similar to that of the Ref specimens. In contrast, a remarkable decrease in crack width (about 50%) was characterised on NE_3% specimens with crack widths less than 300 μm as shown in Fig. 13c. As for cracked specimens containing 3% SH-CS (Fig. 13d), most cracks with crack widths between 150–300 μm were completely healed

after 28 d of water curing. Nevertheless, the self-healing ability of both specimens decreased significantly when the crack width exceeded 300 μm.

Fig. 14 summarised the average crack sealing ratio of mortar specimens containing various types of cenospheres after 7 and 28 d of water-based healing. In comparison to NE_3% and SH_3%, the Ref specimens exhibited the lowest crack sealing ratio, indicating that sodium silicate played a significant role in effectively crack healing in cementitious material, aligning with conclusions drawn in a previous study [20]. Furthermore, up to 71% of the crack-opening area in SH_3% was sealed with the healing product, which is significantly higher than that of NE_3%, P_3% and Ref samples, respectively. This result strongly suggests that including prepared SH-CS facilitates the excellent self-healing capacity of cement mortar.

To visually demonstrate the self-healing effects of different mixtures, changes in the crack mouth area were recorded using optical microscopy (OM). Fig. 15 displays typical images captured at marked positions of the cracked Ref, P_3%, NE_3%, and SH_3% specimens before and after exposure to water healing for 7 and 28 d. On the Ref, P_3%, and NE_3% specimens, crack closure behaviour is not evident, as only a limited area at the crack mouth displayed signs of sealing through the precipitation of repair products. In contrast, the crack opening area of the SH_3% specimens were completely healed after 28 d of water healing. Additionally, in line with the trend depicted in Fig. 14, the crack-sealing effect of specimens containing SH-CS became more pronounced as the healing time extended from 7 to 28 d.

While the images in Fig. 15 showed the effect of SH-CS in sealing cracks at the opening area, the crack-filling capacity remains unclear. In fact, the crack-filling capacity, often overlooked in existing research, is a vital parameter in assessing self-healing performance in cementitious materials [20,58]. Fig. 16 illustrates the morphology of fracture surfaces for various mixtures after 28 d of water healing, and the corresponding repaired area relative to the total fracture surface area is quantified in Fig. 17.

In Fig. 16a and b, the repairing products precipitated on Ref and P_3% specimens are primarily concentrated around the crack opening area, constituting only 26% and 28% of the entire cross-sectional area. These healing products are believed to mainly consist of $CaCO_3$ precipitation. As for NE_3% (Fig. 16c), due to the insufficient supply of Na_2SiO_3 resulting from a lack of encapsulation, the repaired area covered not up to 50% of the fracture surface. In contrast, the repair products of the SH_3% specimens (Fig. 16d) are uniformly distributed across the fracture surface, accounting for 95% of the fracture surface area, as displayed in Fig. 17. The formation of healing products can be attributed to the release of SiO_3^{2-} ions from the evenly dispersed SH-CS and their reaction with portlandite present in the cement hydration products.

4.6.3. Water absorption

Water absorption is a critical parameter for assessing the durability of concrete and has also been employed in evaluating the self-healing efficacy of fractured concrete [59]. Fig. 18 displays the cumulative water absorption results for the Ref specimens and those specimens containing P-CS, SH-CS, and NE-CS after 28 d of water curing. After 4 h of the water absorption test, the Ref specimens exhibited the highest rate of water absorption compared to the specimens incorporating SH-CS and NE-CS. The calculated sorptivity index values for Ref, P_3%, NE_3%, and SH_3% were 0.132, 0.123, 0.109, and 0.079, respectively. This indicates that the inclusion of SH-CS, by substituting 3% of sand in the mixture, resulted in a substantial 41% reduction in the water absorption index value. This reduction can be ascribed to the presence of repair products formed within the cracks, which have a positive effect on decreasing the water adsorption index. Furthermore, the calculated water adsorption index of NE_3%, 0.109, is lower than that of Ref, which can be attributed to the partial filling of the pores and cracks in the mortar matrix due to the release of sodium silicate from the unencapsulated cenospheres and
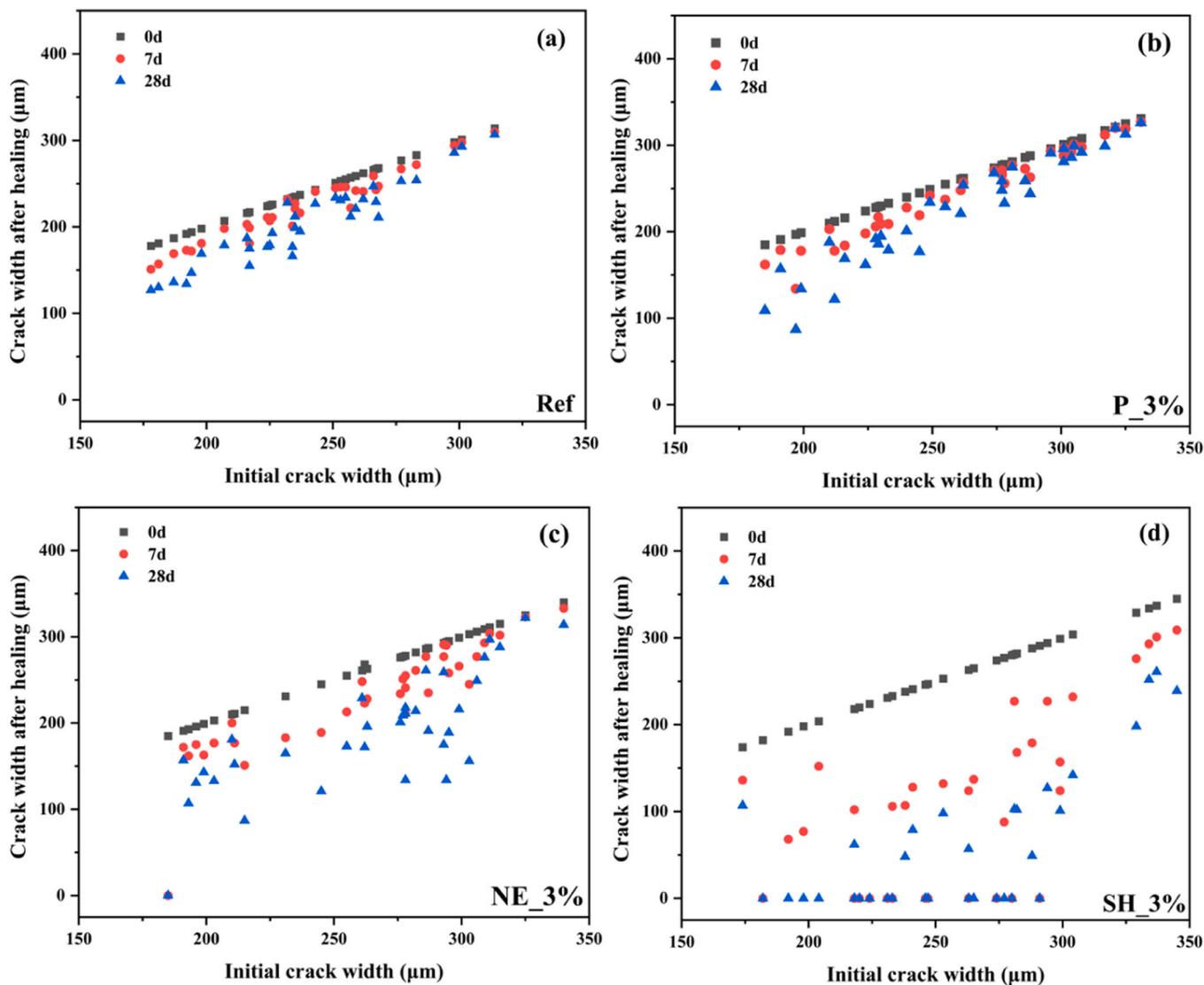
Fig. 13. Crack sealing effect of (a) Ref (b) P_3% (c) NE_3% and (d) SH_3% at different crack widths.
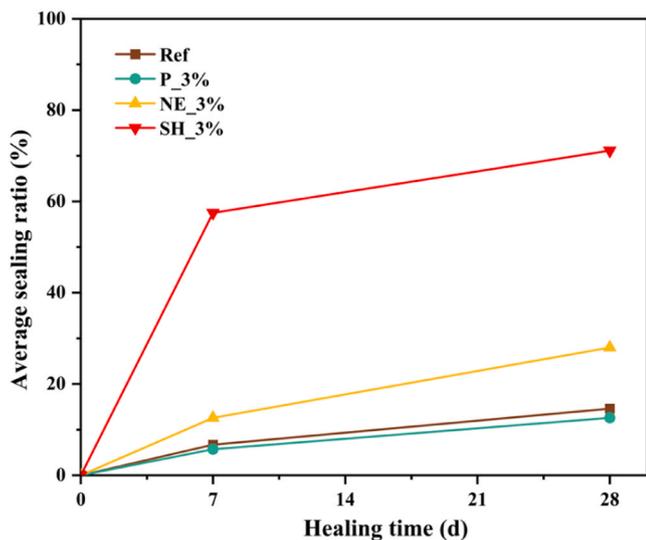

Fig. 14. Average crack sealing ratio of different specimens after healing for 7 and 28 d.

the formation of C-S-H gel.

4.6.4. Mechanical recovery

Fig. 19 presents the flexural strength data obtained from three-point bending tests for various groups of mixtures. The terms "1st round strength" and "2nd round strength" refer to the flexural strength of the intact specimens and the flexural strength of the cracked specimens after healing, respectively. Based on the results of the first-round tests, the inclusion of P-CS and SH-CS had a limited influence on the flexural strength of the mortar. The flexural strength of the Ref group was approximately 9.1 MPa, which was equivalent to that of the P_3% and SH_3% specimens. Notably, the flexural strength of NE_3% was only 7.6 MPa, indicating a 16% decrease compared to the Ref. The sodium silicate released from NE-CS was believed to offset the negative effect caused by the inclusion of cenosphere [33]. In the second-round test, the residual flexural strength resulted from the self-healing effect, and the pull-out strength of pre-embedded steel bars was measured. The residual flexural strength of SH_3% was 5.6 MPa, which is significantly higher than the residual strength of the Ref sample (3.67 MPa). This implies that the self-healing effect of SH-CS contributing to 22% of this strength recovery. It is consistent with a previous finding that an optimal 18% flexural strength recovery in concrete after 28 d of healing using poly-ethylene glycol granule capsules [60].
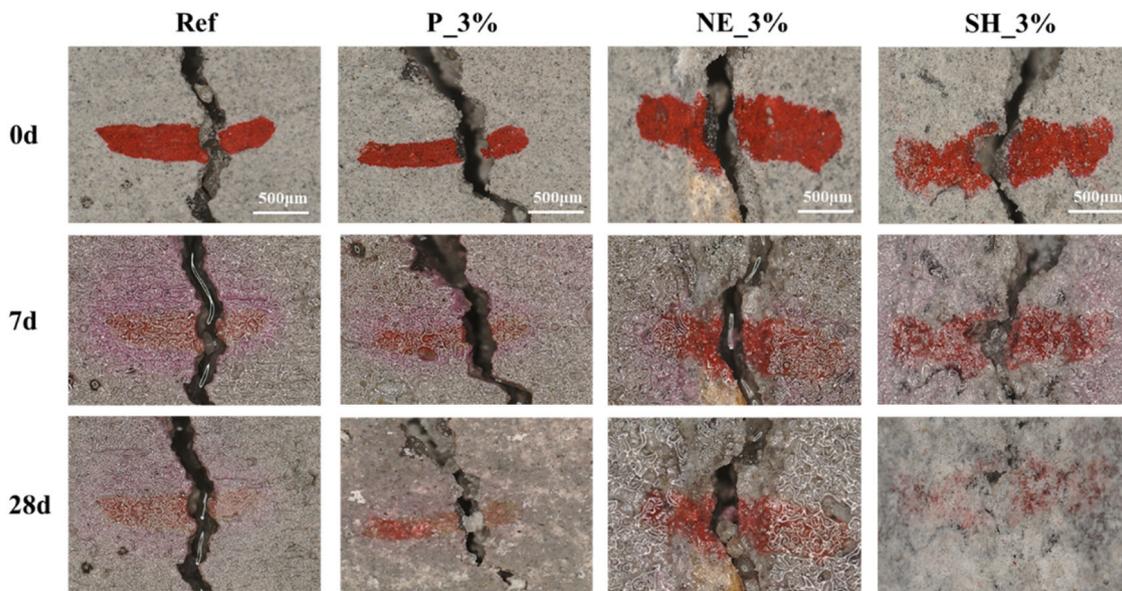
Fig. 15. Cracked opening area of different specimens at healing periods of 0, 7 and 28 d.
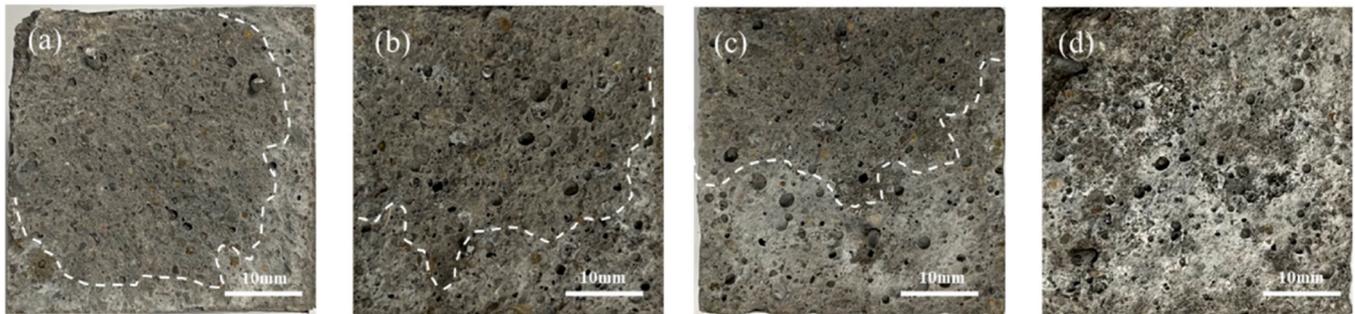

Fig. 16. Fracture surface of (a) Ref, (b) P_3%, (c) NE_3% and (d) SH_3% after the specimens were cured in water for 28 d.
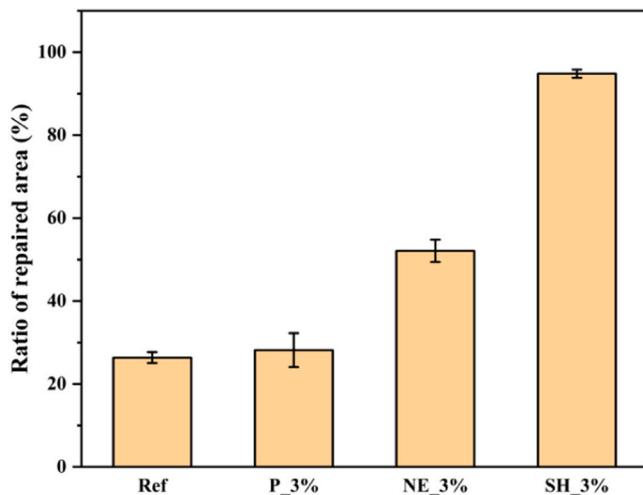

Fig. 17. Average repaired area of the fractured surface of Ref, P_3%, NE_3%, SH_3% after healing in water for 28 d.
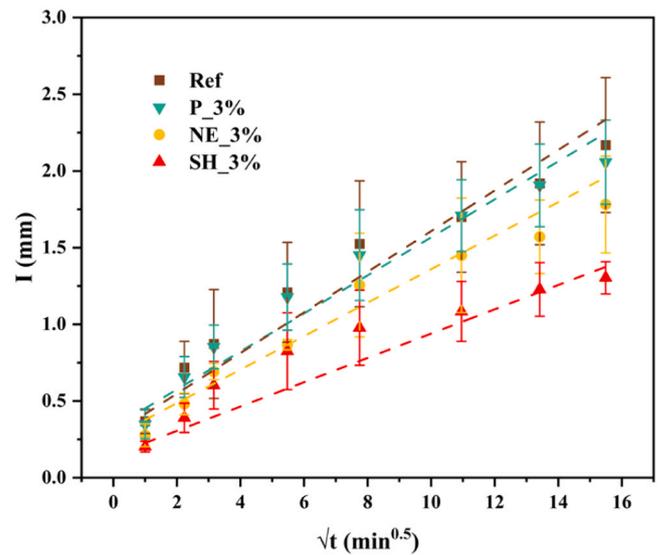

Fig. 18. Cumulative water absorption of the cracked mortar specimens before and after the healing of cracks.

4.6.5. Healing mechanism

To explore the healing mechanism of SH-CS in cementitious materials, the mineral composition of the repairing products collected on the fracture surfaces was analysed using XRD, the results are shown in Fig. 20. The predominant mineral crystal phases formed within the self-

healing products consist of quartz, portlandite and calcite. It is worth noting that due to the inadvertent inclusion of gravel during the collection of repaired products, characteristic peak of quartz was
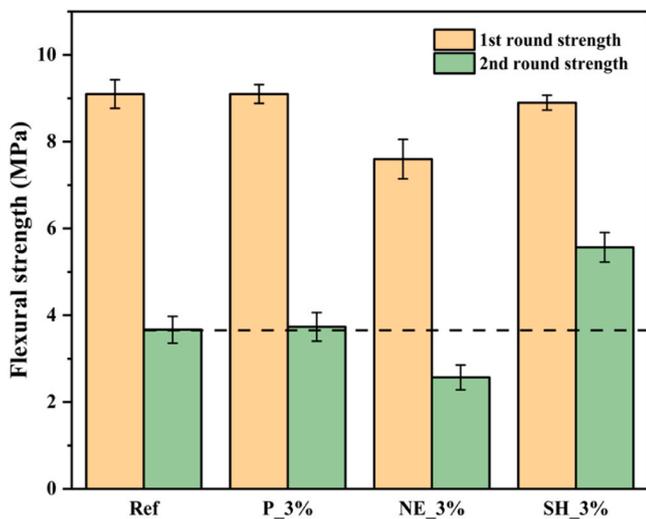
Fig. 19. Flexural strength of mortar samples before and after healing.
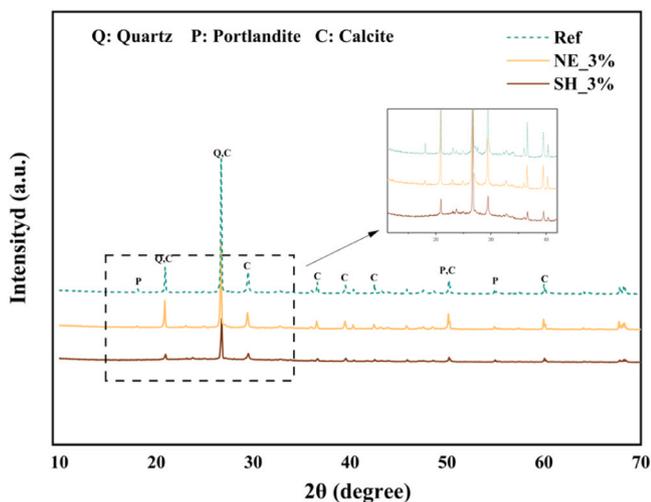

Fig. 20. XRD diffractograms for all healing products.

detected in all repair products, in consistent with that reported in literature [14]. Additionally, the diffraction peak at 2θ= 30° which corresponds to calcite, was evident in all specimens. This can be attributed to the carbonation of calcium hydroxide during the healing process. Remarkably, the intensity of the calcite peak in SH_3% was lower than that observed in the Ref and NE_3% samples. This observation is ascribed to the formation of C-S-H gel through a synthetic reaction between calcium hydroxide and sodium silicate that reduced calcium hydroxide available for carbonation. This reduction aligns with the weaker peak intensity of calcium hydroxide, as evidenced by the diffraction peak of SH_3% at 2θ = 51°in. The characteristic peak of C-S-H were not discernible in the XRD patterns due to its poor crystalline nature. However, as indicated in the magnified portion of the figure, a broad hump-shaped peak between 18–35° was only evident in the XRD patterns of SH_3%. This was believed to correspond to the amorphous phase of C-S-H gel, as reported in previous research[61].

To further analysis of the mineral composition, TG and its derivate coefficient (DTG) curves of the healing product were measured and plotted in Fig. 21. The mass loss in the range of 50 to 200 °C generally relates to the dehydration of ettringite and the evaporation of chemically bound water in the C-S-H gel layer [62]. Comparing SH_3% with the Ref and NE_3% samples, a notable mass loss between 150–230 °C was observed in SH_3%, suggesting the presence of a higher amount of C-S-H gel in the healing product. This observation aligns with the XRD pattern displayed in Fig. 22, where a broad peak associated with C-S-H was evident in SH_3%. The mass loss occurring between 450 to 600 °C is generally attributed to the decomposition of metastable calcium carbonate [63]. Additionally, some researchers have linked the weight loss peak at around 580 °C to the decomposition of C-S-H [64]. Given that the weight loss of SH_3% within the 450–600 °C range is significantly greater than that of the Ref and NE_3%, it is deduced to the decomposition of interlayered calcium carbonate within the C-S-H structure. The mass loss within the 600–750 °C range results from the decomposition of well-crystallized calcium carbonate. The intensity of the weight loss peak in this range follows the order of Ref, NE_3%, and SH_3%, which corresponds to the observations in the XRD pattern.

Fig. 22 shows the FTIR spectra of the healing products collected from Ref, NE_3%, and SH_3%. Characteristic spectral bands associated with the C-O stretching bond are characterized in the range of 870–890 cm^{-1} and 1400–1500 cm^{-1}. These spectral bands are indicative of the presence of carbonate phases in the healing products. Additionally, the spectral band corresponding to Si-O stretching was observed in the range of 950–1100 cm^{-1}, suggesting the existence of calcium silicate
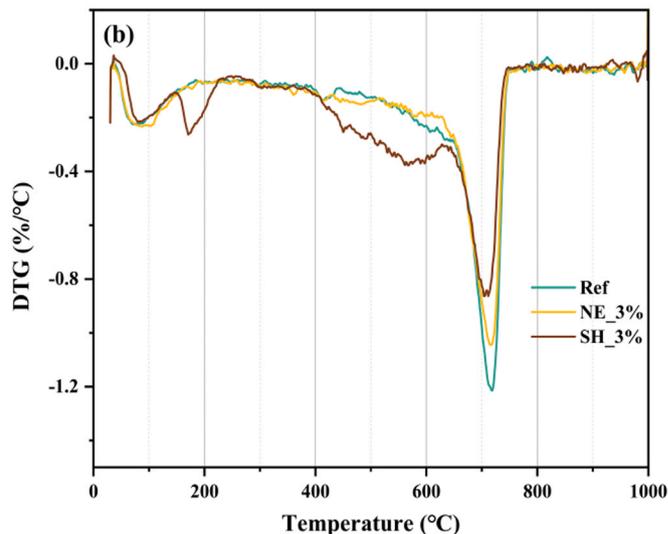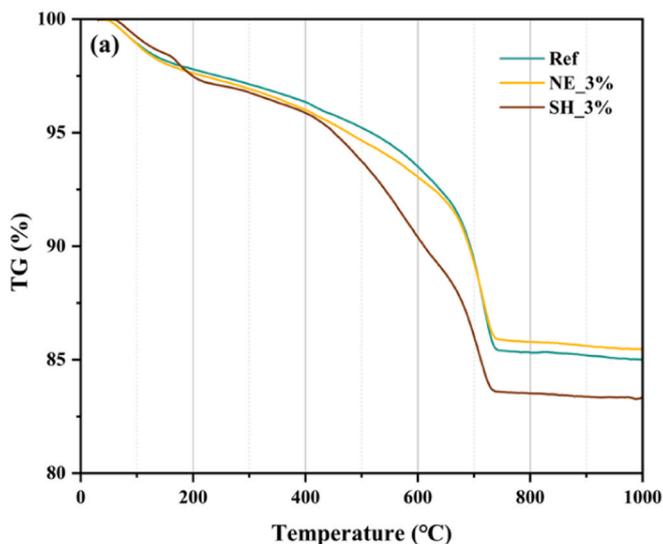

Fig. 21. (a) TG and (b) DTG of the healing products developed in specimens stored under water.
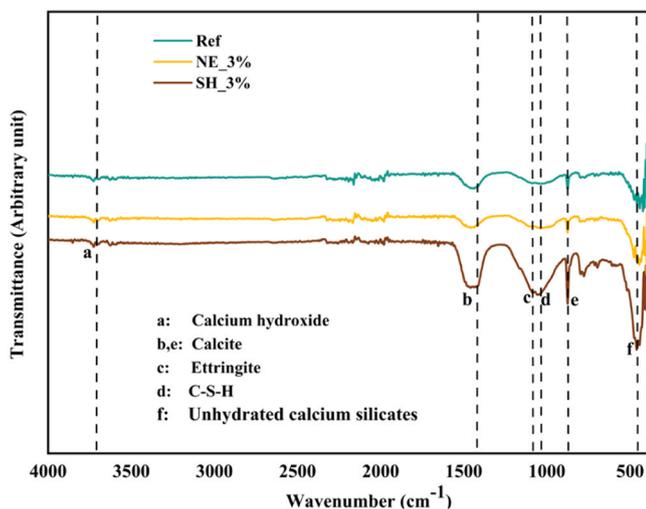
Fig. 22. FTIR spectra of the healing products developed in specimens stored under water.

hydrate (C-S-H) in the samples. Notably, the stretching band of Si-O in the healing products of SH_3% (SH_3%: 1016 cm^{-1}) was more significant compared to the Ref and NE_3% samples (Ref: 979 cm^{-1}, NE_3%: 987 cm^{-1}). As per previous reports [65,66], a higher wavenumber for the Si-O stretching bands implies a higher degree of polymerization within the silicate chain and a greater content of SiO$_2$. These findings further validate the formation of the healing product, C-S-H, on the fracture surface of SH_3%. It should be noted that quantitative analysis is not feasible based on the FTIR results.

The healed crack surface was then observed in the ESEM to characterise the microstructure of the crack surface embedded with SH-CS and NE-CS, respectively. As shown in Fig. 23a, the interlayer transition zone (ITZ) between the SH-CS and cement matrix exhibits a continuous and cohesive texture with the precipitation of fibrous products. This product was believed to be the formation of the healing product, C-S-H, as described in Eq. 1. Besides, sheet-like particles have also been observed in Fig. 23(b), which is associated with the formation of calcite crystals. On the other hand, compared with SH-CS (Fig. 23a), NE-CS showed worse binding with the cement matrix as an interlayer gap can be observed in Fig. 23c. Moreover, cellular-like C-S-H product is not visible in Fig. 23d. This can be inferred that the applied lithium silicate coating not only effectively prevents the leakage of healing agents during mixing but also enhances the bonding between the conosphere and the cement matrix. These observations are in alignment with the results obtained from XRD (Fig. 20), TG (Fig. 21) and FTIR (Fig. 22), indicating that the inclusion of SH-CS contributes to the formation of healing products, C-S-H gel and calcite within the cracked specimens. The schematic diagram of the healing process is displayed in Fig. 24.

4.7. Cost analysis

This study aimed to enhance the cost-effectiveness of existing self-healing concrete solutions. Consequently, a cost analysis of SH-CS and the corresponding self-healing concrete was conducted to establish a benchmark for potential large-scale implementation of this technology in practical engineering applications. The results of the analyses are summarized in Table 5 and Table 6. The calculation is based on the manufacturing procedure described in Section 2.2. The energy and equipment costs have yet to be included in this section. As shown in Table 6, although the cost of producing the SH-CS is significantly higher than the natural river sand, the calculated overall cost of self-healing concrete with 3 wt.$_{sand}$% of SH-CS has increased by 100 CNY/m^3, which is about 22% higher than the standard C40 concrete. Considering its apparent self-healing effectiveness and minor loss in performance, the increase in cost is acceptable for large-scale applications of concrete with high cracking control demands. It must be noted that the precise calculation of the cost is difficult due to the regional differences in material prices.
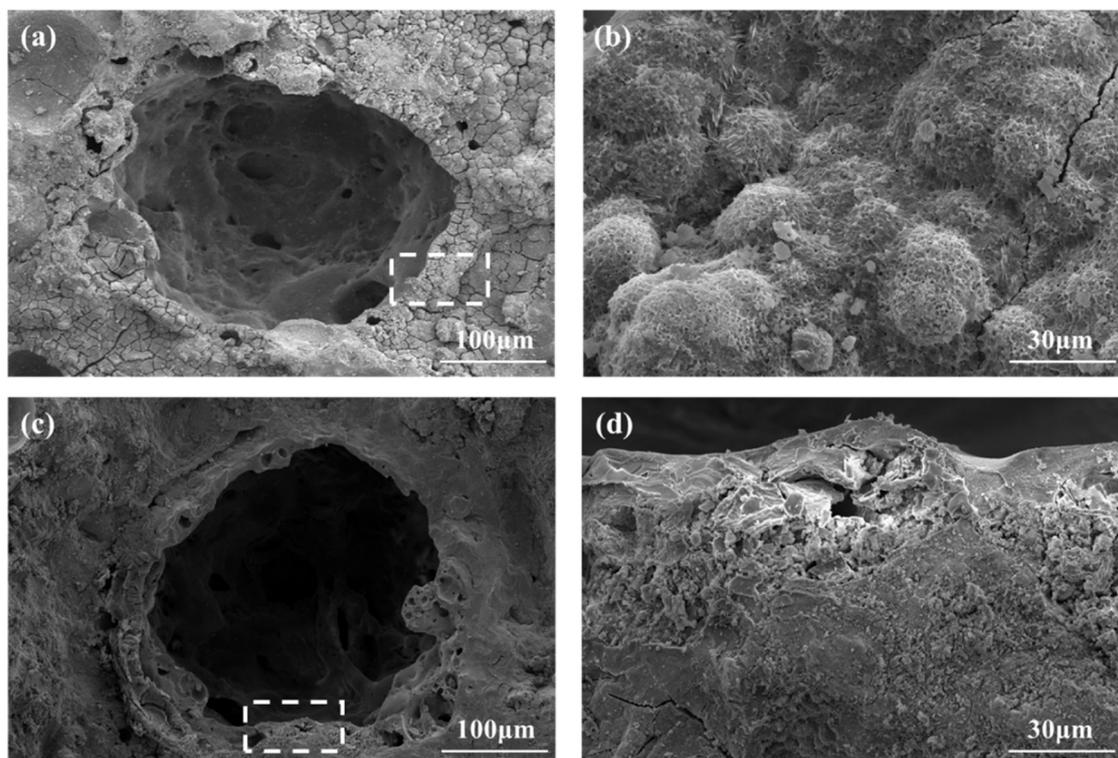

Fig. 23. ESEM images of the healed surfaces embedded with SH-CS (a, b) and NE-CS (c, d). The images on the right (b, d) are the enlarged images of the dash box on the left (a, c).
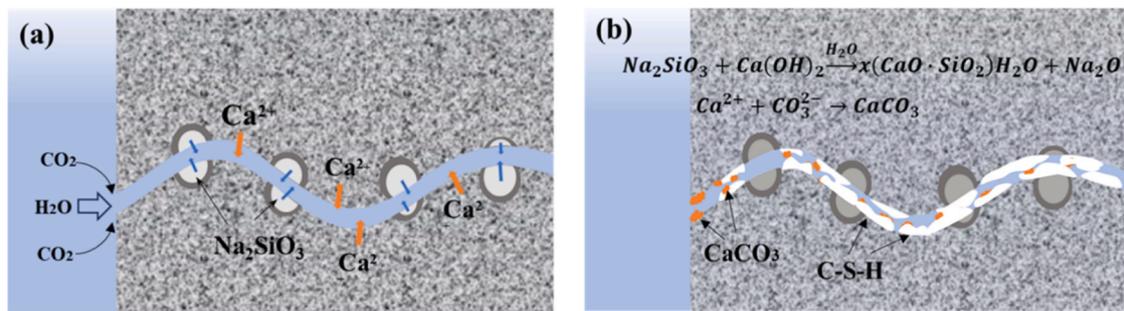
Fig. 24. Schematic diagram of the self-healing process with SH-CS. (a) Cracking in mortar results in the release of Na_2SiO_3 from the SH-CS; (b) reaction between Ca^{2+} with SiO_3^{2-} and CO_3^{2-} leads to the precipitation of $CaCO_3$ and C-S-H gel in the cracking area.

Table 5
Cost estimation of SH-CS.

Raw materials	Unit price (CNY/kg)	Usage amount (kg)	Cost (CNY/kg)
Cenospheres	1.5	0.6	0.9
Hydrofluoric acid	2	1.8	3.6
Sodium silicate	0.8	1	0.8
Lithium silicate	8	0.17	1.36
SH-CS			6.6

Table 6
Cost estimation of self-healing concrete containing 3 wt.$_{sand}$% of SH-CS.

Raw materials	Unit price (CNY/kg)	Cost (CNY/m^3)	
		Normal concrete (C40)	Self-healing concrete
Cement	0.2	450	550
Gravel	0.14		
Water	0.004		
Sand	0.35		
SH-CS	6.6		

5. Conclusions

In this paper, sustainable manufactured aggregate (SH-CS) that employs waste-derived hollow cenospheres as carriers of healing agent was developed through a three-step fabrication process. Based on the experimental results, the following conclusions can be drawn:

(1) The mean particle size of the prepared SH-CS is about 0.5-1.0 mm, i.e., within the size distribution of fine natural aggregate. This enables SH-CS to be used in mortar or concrete as partial replacement for fine aggregate (i.e., sand). The incorporation of SH-CS had a minor effect on the hydration heat, setting time and compressive strength of cement mortar. The setting time and compressive strength were reduced to only about 0.5 h and 4.7% by replacing 3 wt.% sand with SH-CS in the mixture.

(2) By replacing 3 wt.% of sand in the mixture with prepared SH-CS, up to 71.12% of the cracking area in mortar with a crack width of 0.3 mm could be sealed and as much as 95% of the fractured surface was covered through the release of sodium silicate, followed by the formation of C-S-H in the crack space. In addition, the inclusion of SH-CS led to around 41% drop in the water adsorption index. Although the flexural strength of SH_3% was found to decrease by 2.3% with the inclusion of SH-CS, a maximum of 63% of its original flexural strength (8.9 MPa) could be achieved, of which SH-CS contributed 22% to this strength recovery.

(3) The self-healing products formed on the fracture surface during the healing process mainly comprised C-S-H and Calcite.

Amorphous C-S-H gel was produced with the consumption of portlandite and sodium silicate.

(4) The cost of SH-CS products on a large scale is estimated to be about 6.6 CNY per kg which only goes up by about 29% of the price of the concrete per cubic meter. Considering the excellent performance of SH-CS in crack sealing, the proposed self-healing manufactured aggregate has great potential for practical application in large-scale concrete structures.

Although the prepared SH-CS manufactured aggregates with high cost-effectiveness have shown great potential in enhancing the durability of cementitious materials, the self-healing effect was only significant to cracks less than 0.3 mm in this study. This is expected to be overcome by better proportion of the Ca/Si ratio in the fractured microregion through materials design. In addition, field studies should be conducted in actual concrete structures exposed to natural environments.

CRediT authorship contribution statement

Zhu Jihua: Supervision, Funding acquisition. **Xing Feng:** Supervision, Funding acquisition. **Zhang Honghzhi:** Writing – original draft, Methodology. **Pei Chun:** Formal analysis. **Han Kaihang:** Validation, Data curation. **Šavija Branko:** Writing – review & editing. **Zhang Mingzhong:** Writing – review & editing. **Lv Leyang:** Writing – original draft. **Zhang Xiangyu:** Methodology.

Declaration of Competing Interest

The authors declare that they have no known competing financial interests or personal relationships that could have appeared to influence the work reported in this paper.

Data availability

Data will be made available on request.

References

[1] B. Šavija, E. Schlangen, J. Pacheco, S. Millar, T. Eichler, G. Wilsch, Chloride ingress in cracked concrete: a laser induced breakdown spectroscopy (LIBS) study, J. Adv. Concr. Technol. 12 (10) (2014) 425–442.

[2] G.D. Schutter, Quantification of the influence of cracks in concrete structures on carbonation and chloride penetration, Mag. Concr. Res 51 (6) (1999) 427–435.

[3] A. Blagojevi, The Influence of Cracks on the Durability and Service Life of Reinforced Concrete Structures in relation to Chloride-Induced Corrosion, 2016.

[4] D. Carolyn, Matrix cracking repair and filling using active and passive modes for smart timed release of chemicals from fibers into cement matrices, Smart Mater. Struct. 3 (2) (1994) 118.

[5] C.M. Dry, Three designs for the internal release of sealants, adhesives, and waterproofing chemicals into concrete to reduce permeability, Cem. Concr. Res 30 (12) (2000) 1969–1977.

[6] H.M. Jonkers, A. Thijssen, G. Muyzer, O. Copuroglu, E. Schlangen, Application of bacteria as self-healing agent for the development of sustainable concrete, Ecol. Eng. 36 (2) (2010) 230–235.

[7] V.C. Li, Y.M. Lim, Y.-W. Chan, Feasibility study of a passive smart self-healing cementitious composite, Compos. Part B Eng. 29 (6) (1998) 819–827.

[8] N. De Belie, E. Gruyaert, A. Al-Tabbaa, P. Antonaci, C. Baera, D. Bajare, A. Darquennes, R. Davies, L. Ferrara, T. Jefferson, C. Litina, B. Miljevic, A. Otlewska, J. Ranogajec, M. Roig-Flores, K. Paine, P. Lukowski, P. Serna, J.-M. Tulliani, S. Vucetic, J. Wang, H.M. Jonkers, A review of self-healing concrete for damage management of structures, Adv. Mater. Interfaces 5 (17) (2018) 1800074.

[9] P. Minnebo, G. Thierens, G. De Valck, K. Van Tittelboom, N. De Belie, D. Van Hemelrijck, E. Tsangouri, A novel design of autonomously healed concrete: towards a vascular healing network, Materials (2017).

[10] Z. Wan, Z. Chang, Y. Xu, B. Šavija, Optimization of vascular structure of self-healing concrete using deep neural network (DNN), Constr. Build. Mater. 364 (2023) 129955.

[11] Z. Wan, Y. Xu, Y. Zhang, S. He, B. Šavija, Mechanical properties and healing efficiency of 3D-printed ABS vascular based self-healing cementitious composite: experiments and modelling, Eng. Fract. Mech. 267 (2022) 108471.

[12] L. Lv, Z. Yang, G. Chen, G. Zhu, N. Han, E. Schlangen, F. Xing, Synthesis and characterization of a new polymeric microcapsule and feasibility investigation in self-healing cementitious materials, Constr. Build. Mater. 105 (2016) 487–495.

[13] J. Wang, K. Van Tittelboom, N. De Belie, W. Verstraete, Use of silica gel or polyurethane immobilized bacteria for self-healing concrete, Constr. Build. Mater. 26 (1) (2012) 532–540.

[14] A. Kanellopoulos, T.S. Qureshi, A. Al-Tabbaa, Glass encapsulated minerals for self-healing in cement based composites, Constr. Build. Mater. 98 (2015) 780–791.

[15] B. Van Belleghem, S. Kessler, P. Van den Heede, K. Van Tittelboom, N. De Belie, Chloride induced reinforcement corrosion behavior in self-healing concrete with encapsulated polyurethane, Cem. Concr. Res. 113 (2018) 130–139.

[16] J.Y. Wang, H. Soens, W. Verstraete, N. De Belie, Self-healing concrete by use of microencapsulated bacterial spores, Cem. Concr. Res 56 (2014) 139–152.

[17] X. Wu, H. Huang, H. Liu, Z. Zeng, H. Li, J. Hu, J. Wei, Q. Yu, Artificial aggregates for self-healing of cement paste and chemical binding of aggressive ions from sea water, Compos. Part B: Eng. 182 (2020) 107605.

[18] B. Hilloulin, K. Van Tittelboom, E. Gruyaert, N. De Belie, A. Loukili, Design of polymeric capsules for self-healing concrete, Cem. Concr. Comp. 55 (2015) 298–307.

[19] V. Wiktor, H.M. Jonkers, Quantification of crack-healing in novel bacteria-based self-healing concrete, Cem. Concr. Comp. 33 (7) (2011) 763–770.

[20] R. Alghamri, A. Kanellopoulos, A. Al-Tabbaa, Impregnation and encapsulation of lightweight aggregates for self-healing concrete, Constr. Build. Mater. 124 (2016) 910–921.

[21] Y. Su, F. Li, Z. He, C. Qian, Artificial aggregates could be a potential way to realize microbial self-healing concrete: an example based on modified ceramsite, J. Build. Eng. 35 (2021) 102082.

[22] T. Zheng, Y. Su, C. Qian, H. Zhou, Low alkali sulpho-aluminate cement encapsulated microbial spores for self-healing cement-based materials, Biochem. Eng. J. 163 (2020) 107756.

[23] L. Lv, E. Schlangen, Z. Yang, F. Xing, Micromechanical properties of a new polymeric microcapsule for self-healing cementitious materials, Materials (2016).

[24] L.Y. Lv, P.Y. Guo, F. Xing, N.X. Han, Trigger efficiency enhancement of polymeric microcapsules for self-healing cementitious materials, Constr. Build. Mater. 235 (2020).

[25] R.A. Khushnood, Z.A. Qureshi, N. Shaheen, S. Ali, Bio-mineralized self-healing recycled aggregate concrete for sustainable infrastructure, Sci. Total Environ. 703 (2020) 135007.

[26] A. Hanif, Z. Lu, Z. Li, Utilization of fly ash cenosphere as lightweight filler in cement-based composites – a review, Constr. Build. Mater. 144 (2017) 373–384.

[27] D. Montgomery, S. Diamond, The influence of fly ash cenospheres on the details of cracking in flyash-bearing cement pastes, Cem. Concr. Res 14 (6) (1984) 767–775.

[28] A. Hanif, P. Parthasarathy, H. Ma, T. Fan, Z. Li, Properties improvement of fly ash cenosphere modified cement pastes using nano silica, Cem. Concr. Compos. 81 (2017) 35–48.

[29] A. Hanif, P. Parthasarathy, Z. Lu, M. Sun, Z. Li, Fiber-reinforced cementitious composites incorporating glass cenospheres – mechanical properties and microstructure, Constr. Build. Mater. 154 (2017) 529–538.

[30] A. Adesina, Sustainable application of cenospheres in cementitious materials – overview of performance, Dev. Built Environ. 4 (2020) 100029.

[31] F. Liu, J. Wang, X. Qian, Integrating phase change materials into concrete through microencapsulation using cenospheres, Cem. Concr. Compos. 80 (2017) 317–325.

[32] P. Chen, J. Wang, F. Liu, X. Qian, Y. Xu, J. Li, Converting hollow fly ash into admixture carrier for concrete, Constr. Build. Mater. 159 (2018) 431–439.

[33] F. Liu, J. Wang, X. Qian, J. Hollingsworth, Internal curing of high performance concrete using cenospheres, Cem. Concr. Res 95 (2017) 39–46.

[34] J. Giro-Paloma, M. Martínez, L.F. Cabeza, A.I. Fernández, Types, methods, techniques, and applications for microencapsulated phase change materials (MPCM): a review, Renew. Sustain. Energy Rev. 53 (2016) 1059–1075.

[35] M. Hunger, A.G. Entrop, I. Mandilaras, H.J.H. Brouwers, M. Founti, The behavior of self-compacting concrete containing micro-encapsulated phase change materials, Cem. Concr. Compos. 31 (10) (2009) 731–743.

[36] A. Sidiq, R. Gravina, F. Giustozzi, Is concrete healing really efficient? a review, Constr. Build. Mater. 205 (2019) 257–273.

[37] T. EN, 196-1. Methods of testing cement–Part 1: determination of strength, Eur. Comm. Stand. (26 () (2005).

[38] C. ASTM, 1702-09 Standard Test Method for Measurement of Heat of Hydration of Hydraulic Cementitious Materials Using Isothermal Conduction Calorimetry, ASTM International: West Conshohocken, PA, USA, 2009.

[39] C. Astm, 1437, Standard Test Method for Flow of Hydraulic Cement Mortar, Annual Book of ASTM Standards; 2019.

[40] Y. Zhao, X. Hu, C. Shi, Q. Yuan, D. Zhu, Determination of free chloride in seawater cement paste with low water-binder ratio, Cem. Concr. Compos. 124 (2021) 104217.

[41] B. EN, 12620. Aggregates for concrete. London: British Standards Institution (2002).

[42] A. Standard, C109/C109M-20, 2020,"Standard Test Method for Compressive Strength of Hydraulic Cement Mortars (Using 2-in. or [50-mm] Cube Specimens)", ASTM International, West Conshohocken, PA, 2020, DOI: 10.1520/C0109_C01 09M-20.

[43] ASTM, C1585–13, Standard Test Method for Measurement of Rate of Absorption of Water by Hydraulic-Cement Concretes, ASTM International, West Conshohocken, PA, 2013.

[44] L. Lv, P. Guo, G. Liu, N. Han, F. Xing, Light induced self-healing in concrete using novel cementitious capsules containing UV curable adhesive, Cem. Concr. Compos. (2019) 103455.

[45] D. Krizan, B. Zivanovic, Effects of dosage and modulus of water glass on early hydration of alkali–slag cements, Cem. Concr. Res. 32 (8) (2002) 1181–1188.

[46] A.S. Brykov, V.V. Danilov, V.I. Korneev, A.V. Larichkov, Effect of hydrated sodium silicates on cement paste hardening, Russ. J. Appl. Chem. 75 (10) (2002) 1577–1579.

[47] D.M. Kirby, J.J. Biernacki, The effect of water-to-cement ratio on the hydration kinetics of tricalcium silicate cements: testing the two-step hydration hypothesis, Cem. Concr. Res 42 (8) (2012) 1147–1156.

[48] S.P. McBride, A. Shukla, A. Bose, Processing and characterization of a lightweight concrete using cenospheres, J. Mater. Sci. 37 (19) (2002) 4217–4225.

[49] C. Liu, C. Wang, W. Xiao, J. Wu, M. Gao, Study on the performance of calcined spent waterglass foundry sand in alkali-activated foam concrete, Constr. Build. Mater. 378 (2023) 131151.

[50] V. Ponomar, T. Luukkonen, J. Yliniemi, Revisiting alkali-activated and sodium silicate-based materials in the early works of Glukhovsky, Constr. Build. Mater. 398 (2023).

[51] X.H. Li, R.T. Liu, S.C. Li, C.Y. Zhang, J. Yan, Y.K. Liu, X.B. Sun, P.S. Su, Properties and mechanism of self-healing cement paste containing microcapsule under different curing conditions, Constr. Build. Mater. 357 (2022).

[52] X. Wang, Y. Li, C. Zhang, X. Zhang, Visualization and quantification of self-healing behaviors of microcracks in cement-based materials incorporating fluorescence-labeled self-healing microcapsules, Constr. Build. Mater. 315 (2022) 125668.

[53] C. Litina, A. Al-Tabbaa, First generation microcapsule-based self-healing cementitious construction repair materials, Constr. Build. Mater. 255 (2020) 119389.

[54] T.A. de Oliveira, M.D.G.P. Braganca, I.M. Pinkoski, G. Carrera, The effect of silica nanocapsules on self-healing concrete, Constr. Build. Mater. 300 (2021).

[55] K. Sisomphon, O. Copuroglu, E.A.B. Koenders, Self-healing of surface cracks in mortars with expansive additive and crystalline additive, Cem. Concr. Compos. 34 (4) (2012) 566–574.

[56] J. Gao, P. Jin, Y.Z. Zhang, H. Dong, R.X. Wang, Fast-responsive capsule based on two soluble components for self-healing concrete, Cem. Concr. Comp. 133 (2022).

[57] B.Y. Cao, A. Al-Tabbaa, Reactive MgO-based self-healing slag-cement-bentonite slurry walls, Cem. Concr. Comp. 131 (2022).

[58] Z.X. Hu, X.M. Hu, W.M. Cheng, Y.Y. Zhao, M.Y. Wu, Performance optimization of one-component polyurethane healing agent for self-healing concrete, Constr. Build. Mater. 179 (2018) 151–159.

[59] L.Y. Lv, P.Y. Guo, G. Liu, N.X. Han, F. Xing, Light induced self-healing in concrete using novel cementitious capsules containing UV curable adhesive, Cem. Concr. Comp. 105 (2020).

[60] J.H. Feng, H. Dong, R.X. Wang, Y.L. Su, A novel capsule by poly (ethylene glycol) granulation for self-healing concrete, Cem. Concr. Res. 133 (2020).

[61] H. Seiichi, Y. Kazuo, H. Hiroshi, XRD/Rietveld analysis of the hydration and strength development of slag and limestone blended cement, J. Adv. Concr. Technol. 4 (3) (2006) 357–367.

[62] K. Scrivener, R. Snellings, B. Lothenbach, A Practical Guide to Microstructural Analysis of Cementitious Materials || Glossary; 2015.

[63] E.T. Stepkowska, J.M. Blanes, F. Franco, C. Real, J.L. Pérez-Rodríguez, Phase transformation on heating of an aged cement paste, Thermochim. Acta 420 (1) (2004) 79–87.

[64] Y. He, X. Zheng, L. Lv, S. Yu, G. Deng, S. Hu, Dehydration characteristics of C-S-H with Ca/Si Ratio 1.0 prepared via precipitation, J. Wuhan. Univ. Technol. (3) (2018).

[65] S.-Y. Hong, F.P. Glasser, Alkali sorption by C-S-H and C-A-S-H gels: part II. Role of alumina, Cem. Concr. Res. 32 (7) (2002) 1101–1111.

[66] I. García-Lodeiro, A. Fernández-Jiménez, M.T. Blanco, A. Palomo, FTIR study of the sol–gel synthesis of cementitious gels: C–S–H and N–A–S–H, J. Sol. Gel Sci. Technol. 45 (1) (2008) 63–72.